VECTOR-CONTROLLED CSI-FED INDUCTION MOTOR DRIVES WITH ACTIVE DAMPING LC FILTER RESONANCE

S.Pandimeena & R.Saravanan

Assistant Professors, Department of Electrical and Electronics Engineering, Pandian Saraswathi Yadav Engineering College, Sivagangai, Tamilnadu, India

Abstract

For longer life of alternating-current (ac) machines, it is desirable to feed them by sinusoidal voltages. This can be achieved by connecting an LC filter between the voltage source inverter and the motor. However, the LC filter creates unwanted oscillation at system resonant frequency. A resistance connected in series with the capacitor is a solution to damp out the resonant-frequency oscillation, but this damping technique increases loss in the system. In this paper, a simple active damping technique is proposed for lossless damping of vector-controlled ac motor drives with an LC filter. In the proposed technique, the resistance drop is emulated in the control using the terminal motor voltages. The proposed technique is carried out in the three-phase domain for better accuracy of the control. Important features of the proposed technique are:

1) The control action is taken in per-phase basis for accurate extraction of resonant-frequency signal extraction, which, in turn, ensures appropriate damping.
2) The proposed technique emulates a virtual series resis-tance for AD of the *LC* resonance in the control, only by using the terminal voltage information.
3) The proposed technique corrects the delay in the damping signals caused by the switching action of the VSI.

The proposed technique neither affects the dynamic response of the drive nor changes the design of the standard vector control loops. Results from experimental ac motor drives are presented.

Index Terms—Active damping (AD), induction machine, *LC* filter, synchronous machine, vector control.

I. Introduction

The voltage-source-inverter (VSI)-fed alternating-current (ac) drive topology is standard in the industry. Due to high *dv/dt* of the VSI output voltages, bearing failure, insulation failure of the motor windings, and issues related to electromag-netic compatibility/interference are common [1]–[6]. Passive *dv/dt* filters, common-mode filters, and pulsewidth-modulation (PWM) techniques have been proposed to mitigate the afore-mentioned problems [7]–[11]. However, for longer life of the motor, it is always desirable to operate the machine with sinu-soidal voltages. One common method is to connect an *LC* filter between the inverter and the machine. The *LC* filter smoothens the VSI output voltage and supplies sinusoidal voltage into the motor. However, when ac machines are driven by a VSI with an output *LC* filter, the motor terminal voltage oscillates at system resonant frequency. Although the magnitude of the resonant-frequency voltage in the VSI is small, the *LC* filter does not offer any impedance at the resonant frequency. Therefore, a large amount of resonating current circulates between the VSI and the *LC* filter. The resonating current magnitude is restricted only by the filter resistance. Due to this circulating current, motor voltage also oscillates at the resonant frequency.

The control of such a configuration, when the filter cor-ner frequency is within the bandwidth of the current loops, has been addressed [12]–[15]. Vector control of the induction machine with the *LC* filter is implemented by using four cascaded proportional–integral loops [12]. Capacitor-voltage and inductor-current control loops are present, in addition to the main vector control loops. The active damping (AD) method provides a good alternative solution for this problem. To date, very little work has been reported on AD for VSI-fed adjustable speed drives for ac machines. However, AD with direct torque control has been proposed [16]. In that paper, the correction terms for *LC* resonance are added to the torque.

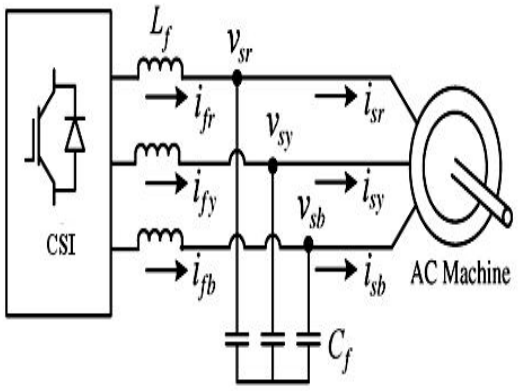

Fig. 1. Power hardware.

The AD technique has been also reported for *LCL*-filter-based grid side converter [17]–[21], [25], [27], [29]–[32], current source inverter with *CL* filter [21], [22], [26], unin-terruptable power supply application [23], and direct-current (dc)–dc converter [24] for good transient and steady-state per-formances.

A simple and robust AD technique for the grid-side con-verter is proposed [17]. In that paper, the antiphase capacitor resonating voltages are subtracted from the voltage references in the synchronous reference frame. However, the phase shift of voltages due to the *LC* filter is not addressed. AD for the grid-side converter using lead–lag compensator was proposed [18]. A genetic-algorithm-based AD technique for the grid-side converter was also proposed [19]. A model predictive control scheme was adopted for the *LCL*-filter-based active front-end converter [27]. AD for the current source converter with a virtual parallel resistor across the capacitor was emulated in the control [22].

In this paper, a simple AD technique is proposed for vector-controlled VSI-fed ac motors.

Important features of the proposed technique are:

- The control action is taken in per-phase basis for accurate extraction of resonant-frequency signal extraction, which, in turn, ensures appropriate damping.
- The proposed technique emulates a virtual series resis-tance for AD of the *LC* resonance in the control, only by using the terminal voltage information.
- The proposed technique corrects the delay in the damping signals caused by the switching action of the VSI.

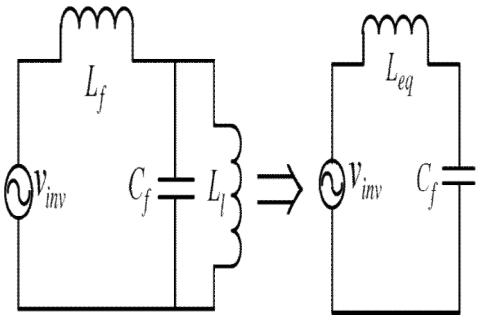

Fig. 2. (a). Equivalent *LC* circuit. (b). Thevenin equivalent of *LC* circuit. DRIVE

- The proposed technique damps out transient voltage oscillations during sudden speed and load change and minimizes steady-state resonant-frequency oscillation
- The proposed AD technique does not affect the main control loops of the field-oriented control; the design of the AD Controller

This paper is organized in the following way: Section II describes the power structure and the brief overview of the proposed control technique. Section III describes the proposed AD technique. Section IV presents the detailed experimental results both for steady state and transient response for induction and synchronous machine, which demonstrates the effectiveness of the proposed technique. Section V summarizes the main points of the paper.

II. Description of the Power Converter Structure and the philosophy of the control technique

A. Description of Power Converter Structure

Fig. 1. shows the power circuit of an ac machine connected to a VSI by an LC filter. Lf is the filter inductance, and Cf is the filter capacitance. vsr, vsy, and vsb are the capacitor voltages; isr, isy, and isb are the machine currents; and ifr, ify, and ifb are the filter currents. Fig. 2(a) and (b) is the equivalent circuits of the ac motor. Ll is the leakage inductance of the machine. For an induction machine, Ll is the sum of the stator (Lls) and rotor (Llr) leakage inductances. For a synchronous machine, Ll is the synchronous inductance Ls of the machine. The equivalent resonating elements are the filter capacitor Cf and the parallel combination of the filter inductance Lf and Ll

For a synchronous machine, the synchronous inductance Ls is large, as compared with the filter inductance Lf . Therefore, the equivalent inductance Leq for the synchronous machine is almost the same magnitude as Lf

For the induction machine

$$Leq = [Lf \times (Lls + Llr)] / [Lf + (Lls + Llr)]$$

Table 1

Filter Details for Induction Machine Drive with Operating Switching Frequency at 2.4 and 4.9 khz

Filter Inductance	L_f	2 mH	0.05 p.u.
Total machine Leakage inductance	$L_{ls}+L_{lr}$	3.24 mH	0.09 p.u.
Filter capacitance	C_f	30 uF	0.2 p.u.
Resonant Frequency	ω_n	828 Hz	16.6 p.u.

Table II

Filter Details for Synchronous Machine Drive

Filter Inductance	L_f	5 mH	0.12 p.u.
Synchronous inductance	L_s	50.2mH	1.25 p.u.
Filter capacitance	C_f	20 uF	0.08 p.u.
Resonant Frequency	ω_n	503 Hz	10.06 p.u.

For the synchronous machine

$$\text{Leq} = (L_f L_S)/(L_f + L_S) \approx L_f . \qquad (2)$$

Equations (1) and (2) are derived by thevinizing the circuit, as shown in Fig. 2(a) and (b).

$$\omega_n = 1/\sqrt{L_{eq} C_f}$$

Around 10% voltage drop is allowed across the filter inductor. The Choice of the inductor value is made as a compromise between reduction of inductor current ripple amplitude and inductor size. The capacitor value can be chosen such that the system resonant frequency ω_n is lesser than one third of the inverter switching frequency [3] This is a tradeoff between the filter size and attenuation of the resonant frequency by the control action. In this case, at least three samples can be obtained to replicate the resonant frequency components. The filter details for an induction motor and a synchronous motor are given in Tables I and II. The machine details are

given in the Appendix

Philosophy of the control Technique

. A Residence can be connected in serious with the capacitor to damp out the L C resonance. This Solution increases power loss in the system. To achieve losses damping , An AD Method is proposed . In the proposed AD Technique, a fictitious resistance value is multiplied by the individual capacitor currents at the resonant frequency and substrated from the source voltages. In this way, a damping effect of the resistance is emulated but in a lossless fashion. The difficulty in this methods is that the capacitor current noisy. The capacitor current consist of switching- frequency components, along with fundamental

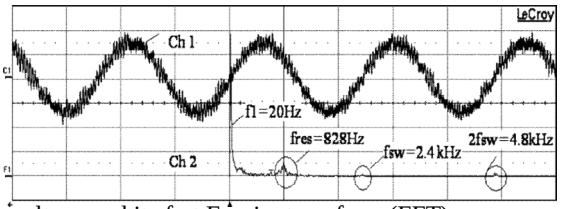

Fig. 3. *R*-phase capacitor voltage and its fast Fourier transform (FFT)
at 20 Hz (inverter switching frequency, 2.4 kHz). Ch1: Capacitor voltage, 50 V/div; time, 20 ms/div; Ch2: FFT of the capacitor voltage (frequency scale, 1 kHz/div; magnitude scale, 10 V/div).

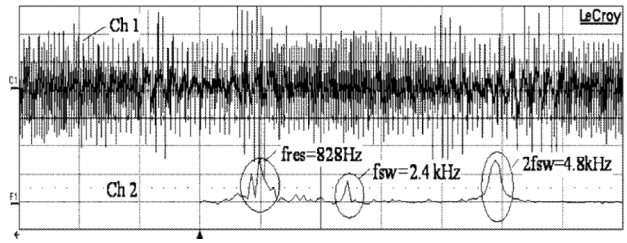

Fig. 4. *R*-phase capacitor current and its FFT at 20 Hz (inverter switching frequency, 2.4 kHz). Ch1: Capacitor current, 10 A/div; time: 5 ms/div; Ch2: FFT of the capacitor current (frequency scale, 1 kHz/div; magnitude scale, 10 A/div).

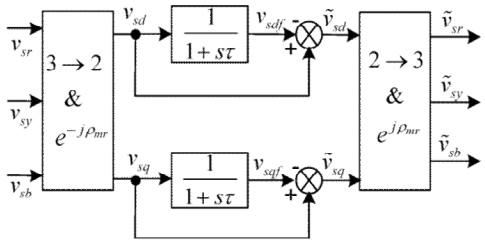

$e^{-j\rho_{mr}}$ =Transformation from stationary coordinate to rotor flux coordinate.
$e^{j\rho_{mr}}$ = Transformation from rotor flux coordinate to stationary coordinate.

Fig. 5. Signal extraction

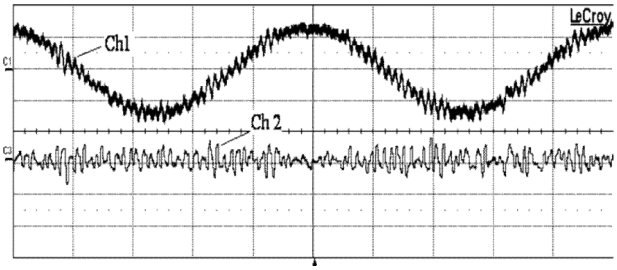

Fig. 6. *R*-phase capacitor voltage and extracted resonant signal $v\tilde{}_{sr}$ at 20 Hz (inverter switching frequency, 2.4 kHz). Ch1: Caacitor voltage, 50 V/div; Ch2: $v\tilde{}_{sr}$, 25 V/div; time, 10 ms/div.

and resonant components. In cases where the resonant and switching frequencies are close by, it will be difficult to extract only the resonant-frequency component from the sensed capac-itor currents. However, when the inverter switching frequency is high (more than 2 kHz), the capacitor *voltage* contains only the fundamental and resonant components (see Fig. 3). It does not contain the significant switching-frequency com-ponent. However, the capacitor *current* contains a consider-able amount of switching-frequency components (see Fig. 4). The switching-frequency component (2.4 kHz) is close to the resonant-frequency component (828 Hz) with higher magnitude (see Fig. 4). These create serious difficulty in extracting only the resonant-frequency component from the sensed capacitor cur-rent, which is required for the control. Therefore, in this paper, it is proposed to emulate the resonant component of the capaci-tor currents with the help of signatures in the capacitor voltages when the inverter switching frequency is more than 2 kHz. In the proposed AD technique, compensation for the inverter delay can be also easily and accurately incorporated. However, when the inverter switching frequency is very low (around 500 Hz), the switching-frequency components in the capacitor voltage are higher in magnitude compared with the resonant frequency. Therefore, in these cases, suitable PWM techniques have to be adopted to reduce the switching-frequency harmonics in the capacitor voltages [28].

III. Description of Control Topology

Exact and noise free, resonant-frequency capacitor volt-ages are essential for the control. In Section III-A, the pro-posed resonant-frequency signal extraction is described. In Section III-B, the procedure to generate compensating signals for the proposed AD technique is discussed.

A. Resonant-Frequency Signal Extraction Block

Fig. 5 describes the resonant-frequency signal extraction block. At the steady state, the machine terminal voltages con-tain fundamental- (ω_f) and resonant-frequency (ω_n) signals. When the switching frequency of the inverter is high (> 2 kHz), the switching-frequency component in the capacitor voltages are comparatively lower in magnitude than the resonant-frequency components (see Fig. 3). Machine-per-phase volt-ages v_{sr}, v_{sy}, and v_{sb} are sensed to extract resonant capacitor voltages. The sensed voltages are transformed into the *d–q* domain. In the transformed *d–q* voltages v_{sd} and v_{sq}, both the fundamental components v_{sdf} and v_{sqf} and the resonant components $v\tilde{}_{sd}$ and $v\tilde{}_{sq}$) are present. v_{sdf} and v_{sqf} are dc quantities and $v\tilde{}_{sd}$ and $v\tilde{}_{sq}$ are ac quantities that

are close to the resonant frequency, i.e.,

$$v_{sd} = v_{sdf} + \tilde{v}_{sd} \quad (4)$$

$$v_{sq} = v_{sqf} + \tilde{v}_{sq}. \quad (5)$$

v_{sd} and v_{sq} are filtered using low-pass filters with cutoff fre-quencies at around 10 Hz. The outputs of the low-pass filters are v_{sdf} and v_{sqf} . They are subtracted from v_{sd} and v_{sq} to extract $\tilde{v}_{sd}$ and $\tilde{v}_{sq}$. The extracted resonant-frequency compo-nents $\tilde{v}_{sd}$ and $\tilde{v}_{sq}$ have frequency $(\omega_n - \omega_f)$ due to the *d–q* transformation. . To get rid of this variation of ω_f in $\tilde{v}_{sd}$ and $\tilde{v}_{sq}$, they are transformed back to the three-phase domain. The outputs of the reverse transform are $\tilde{v}_{sr}$, $\tilde{v}_{sy}$, and $\tilde{v}_{sb}$. Due to the reverse transformation, the extracted-per-phase resonant-frequency capacitor voltages $\tilde{v}_{sr}$, $\tilde{v}_{sy}$, and $\tilde{v}_{sb}$ are exactly at ω_n. Fig. 6 shows the waveform of $\tilde{v}_{sr}$. Most of the AD techniques available in the literature do not compensate in the three-phase domain but in the *d–q* domain [17], [18].Hence,thefrequency

Fig. 7. Inclusion of the virtual resistance in the equivalent *LC* circuit.
(a) Circuit representation. (b) Control block diagram representation.

of the extracted components lies at $(\omega_n - \omega_f)$. Therefore, a little frequency mismatch exists in these techniques.

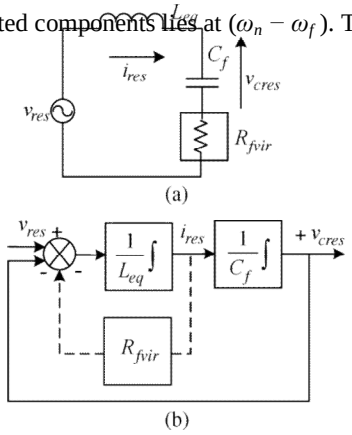

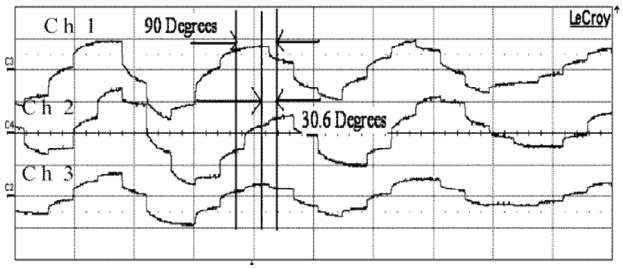

B. LC Filter Control Block

The *LC* filter control block in Fig. 19 demonstrates the proposed AD technique adopted to mitigate the *LC* filter resonance. A series *LC* circuit excited by a sinusoidal voltage source at the resonant frequency does not offer any impedance to the circuit. When a resistance is added in this *LC* circuit, then the current magnitude at the resonant frequency is damped by this resistance. The resistance can be placed in series or in parallel with the capacitor. However, this solution causes power loss in the circuit and reduces efficiency of the drive. Therefore, the AD technique is adopted to damp out the oscillation in lossless fashion without physically connecting any resistance in the circuit.

In the proposed method of AD, a series resistance in the *LC* circuit is emulated in the control. A resistance connected in parallel with the capacitor can be also adopted [22], [26, Sec. 11.5]. However, this technique causes additional delay in the system as the corrective signals have to pass through the current control loops.

Fig. 7(a) shows an *LC* circuit excited by a resonating voltage source v_{res}. A series resistance R_{fvir} is emulated in the control. Fig. 7(b) is the control block diagram of the series *RLC* circuit in Fig. 7(a). The capacitor current i_{res} at the resonant frequency is multiplied by the virtual resistance R_{fvir} and subtracted from the

source voltage v_{res}. It is very straightforward to multiply R_{fvir} with the resonant capacitor current i_{res} to emulate the resistance drop. However, i_{res} contains a considerable amount of switching-frequency components, along with the resonant-frequency component of the current (see Fig. 4). When both of them are close by, it is difficult to extract only the resonat-ing part from the capacitor current signal, but the extracted resonant capacitor voltages $v\tilde{}_{sr}$, $v\tilde{}_{sy}$, and $v\tilde{}_{sb}$ mainly contain the resonant-frequency components (see Fig. 6), and they lag by 90° from the resonating capacitor currents. The extracted resonant capacitor voltages $v\tilde{}_{sr}$, $v\tilde{}_{sy}$, and $v\tilde{}_{sb}$ are integrated to obtain $v\tilde{}_{sr\_int}$, $v\tilde{}_{sy\_int}$, and $v\tilde{}_{sb\_int}$ signals (see Fig. 8). Instead of a pure integrator, a low-pass filter is used to generate $v\tilde{}_{sr\_int}$,

Fig. 8. *R*-phase-extracted capacitor voltage $v\tilde{}_{sr}$, integrated voltage $v\tilde{}_{sr\_int}$, and compensated signal v_{r_comp} at 20 Hz (inverter switching frequency, 4.9 kHz). Ch1: $v\tilde{}_{sr}$, 10 V/div; Ch2: $v\tilde{}_{sr\_int}$, 10 V/div; Ch3: v_{r_comp}, 20 V/div; time, 500 μs/div.

Table III

Inverter Delays Generated at Different Experimental Conditions

Experimental Conditions	*Inverter Delay* $(\omega_n T_s/2)$
Induction Machine, switching freq.=2.4 kHz, Resonant freq.=828 Hz.	61.1°
Induction Machine, switching freq.=4.9 kHz, Resonant freq.=828 Hz.	30.6°
Synchronous Machine, switching freq.=4.9 kHz, Resonant freq.=503 Hz.	18.6°

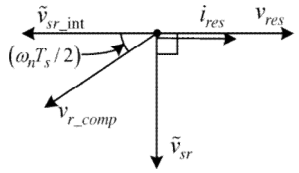

Fig. 9. Phasor description at the resonant frequency for sustained oscillation.

$v\tilde{}_{sy\_int}$, and $v\tilde{}_{sb\_int}$ signals to avoid dc drift problems. The cutoff frequencies of these low-pass filters are kept at around 50 Hz, which are far below the resonant frequency ω_n. There-fore, these low-pass filters do not cause any phase shift to the $v\tilde{}_{sr\_int}$, $v\tilde{}_{sy\_int}$, and $v\tilde{}_{sb\_int}$ signals. These signals lag by 180° out of phase from the resonant capacitor currents. $v\tilde{}_{sr\_int}$ lags by 90° from $v\tilde{}_{sr}$ (see Fig. 8).

In Fig. 8, phasor relationships for $v\tilde{}_{sr}$, $v\tilde{}_{sr\_int}$, and v_{r_comp} are elaborated for an induction motor drive with the inverter switching frequency kept at 4.9 kHz.

When the inverter switching frequency is close to the resonant frequency, the inverter introduces a considerable amount of phase delay to the compensating signals $v\tilde{}_{sr\_int}$, $v\tilde{}_{sy\_int}$, and $v\tilde{}_{sb\_int}$. Therefore, it is essential to advance the phase of $v\tilde{}_{sr\_int}$, $v\tilde{}_{sy\_int}$, and $v\tilde{}_{sb\_int}$ to compensate the inverter phase lag. Table III elaborates the phase delay ($\omega_n T_s/2$) gen-erated by the inverter for the experiments carried out in this paper. The phase delay is predicted from the system resonance and switching frequencies of the inverter.

Fig. 9 shows the phasor relationships of important signals at the resonant frequency. The inverter source voltage v_{res} and the resonant capacitor current i_{res} are in the same phase. The capacitor voltage $v\tilde{}_{sr}$ lags them by 90°. $v\tilde{}_{sr\_int}$, $v\tilde{}_{sy\_int}$, and $v\tilde{}_{sb\_int}$ are at the opposite phase with i_{res}. $v\tilde{}_{sr\_int}$, $v\tilde{}_{sy\_int}$, and $v\tilde{}_{sb\_int}$ signals are phase advanced by $\omega_n T_s/2$ to construct the

TABLE IV
VARIATION OF f_n AND ξ

	$(L_{ls}+L_{lr})$ (3.24mH)	+20% $(L_{ls}+L_{lr})$	−20% $(L_{ls}+L_{lr})$
f_n (Hz)	828	802	894
ξ	0.3	0.29	0.324

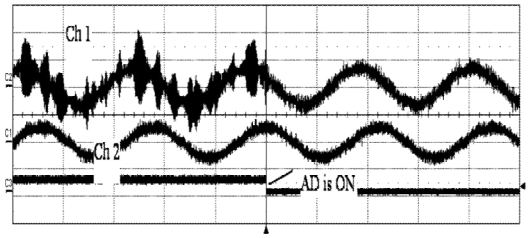

per-phase compensating signals v_{r_comp}, v_{y_comp}, and v_{b_comp}. This phase advancement compensates the delay of $\omega_n T_s/2$ introduced by the inverter. The inverter switching frequency is f_s, and the inverter time constant is $T_s/2$, where $T_s = 1/f_s$. v_{r_comp} is obtained from

$$v_{r\_comp} = v\tilde{}_{sr\_int} \cos(\omega_n T_s/2) + v\tilde{}_{sr} \sin(\omega_n T_s/2). \quad (6)$$

As cos $(\omega_n T_s/2)$ and sin $(\omega_n T_s/2)$ are fixed numbers, the compensation for the inverter delay can be easily and accu-rately introduced. For the proposed AD, v_{r_comp}, v_{y_comp}, and v_{b_comp} signals are multiplied by the scaling factor K_{damp} to emulate the resistance drop, i.e.,

$$v_{invr\_res} = K_{damp} \times v_{r\_comp}. \quad (7)$$

v_{invr_res}, v_{invy_res}, and v_{invb_res} signals are directly added tothe inverter voltage references v_{invr}^*, v_{invy}^*, and v_{invb}^* generated from the standard vector control block. The corrective action is instantaneous as the correcting signals are directly added to the inverter voltage references. Moreover, the proposed AD technique does not hamper the main vector control loops.

K_{damp} can be expressed in terms of the damping factor ξ, i.e.,

$$K_{damp} = R_{fvir} |i_{res}(t)/v_{r\_comp}| = 2\xi \quad (8.a)$$

Where

$$\xi = (R_{fvir}/2) \sqrt{C_f/L_{eq}}. \quad (8.b)$$

Fig. 10. *R*-phase capacitor voltage and machine current at 5 Hz (ξ = 0.3) with and without AD. Ch1: Capacitor voltage, 25 V/div; Ch2: machine current, 20 A/div; time, 100 ms/div.

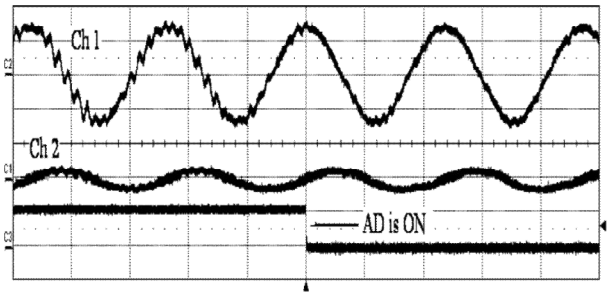

Fig. 11. *R*-phase capacitor voltage and machine current at 43 Hz (ξ = 0.3) with and without AD. Ch1: Capacitor voltage, 125 V/div; Ch2: machine current, 20 A/div; time, 10 ms/div.

fore, small changes in the resonant frequency will not hamper the control action. The variation of ξ will change the value of the damping resistance to be added in the system. However, this small change, as shown in Table IV, will not cause much variation in the proposed damping. Experimental results in Fig. 18(a) and (b) demonstrate the robustness of the proposed damping technique.

It is experimentally observed that, for ξ varying from 0.2 to 0.4, the system most effectively works. For the lower damping factor, the damping effect is not prominent, and for the higher damping factor, the compensating signals cause distortion to the actual voltage signals.

The complete block diagram of the proposed AD technique is shown in Fig. 19. The block diagram is valid for both induction and synchronous machines.

C. System Robustness

The values of the stator and rotor leakage inductances may vary with time, or there may be error in the measurements. To account these changes, ±20% variation of the total stator and rotor leakage inductances is considered. Due to these variations, following changes in the system will happen: 1) The resonant frequency will change. 2) Damping factor ξ will change.

The variation of the resonant frequency f_n and the damping factor ξ due to the variation of the values of the stator and rotor leakage inductances are shown in Table IV.

The extraction of the resonant-frequency signal is not de-cided by any predetermined resonant-frequency value. There-

IV. Experimental results

A. Experimental Results for an Induction Machine (Steady State)

The experiment is carried out using a two-level insulated-gate-bipolar-transistor (IGBT)-based VSI, and the control algo-rithm is implemented on a TMS320LF 2407A digital platform. Machine and filter details are given in the Appendix and in Table I. The inverter switching frequency is kept for these experiments at 2.4 and 4.9 kHz. The system resonant frequency is fixed at 828 Hz. The current controller bandwidths are fixed at 100 Hz. The analog-to-digital converter (ADC) sampling frequency is kept at the switching frequency of the inverter. Anti-aliasing filters with 30-kHz bandwidth are used before the ADC section to remove high-frequency noises from the sensed signals.

Experimental Results at the 4.9-kHz Switching Frequency:

Figs. 10 and 11 are the waveform for the damping factor $\xi = 0.3$. The damping factor decides the magnitude of the resistance to be included in the circuit. Phase advancement given to compensate the inverter delay is 30.6° (as shown is

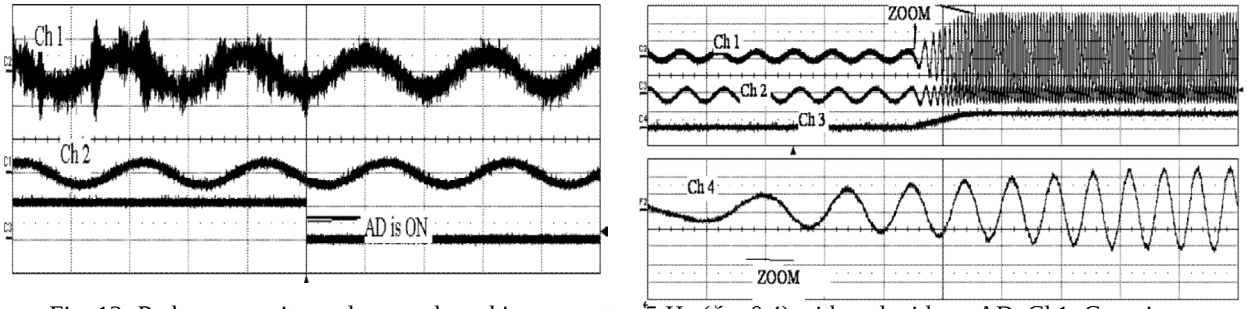

Fig. 12. *R*-phase capacitor voltage and machine current at 5 Hz ($\xi = 0.4$) with and without AD. Ch1: Capacitor voltage, 25 V/div; Ch2: machine current, 20 A/div; time, 100 ms/div.

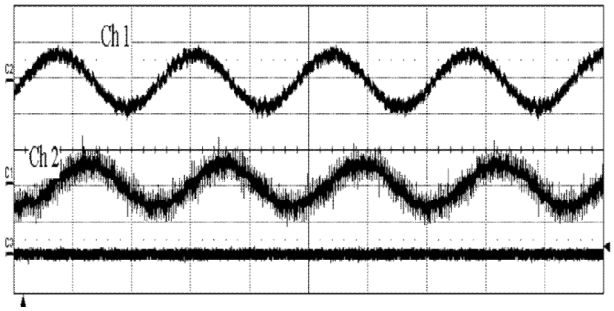

Fig. 13. *R*-phase capacitor voltage and machine current at 43 Hz ($\xi = 0.4$) with AD. Ch1: Capacitor voltage, 125 V/div; Ch2: machine current, 20 A/div; time, 10 ms/div.

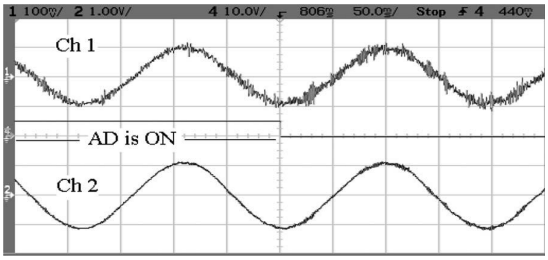

Fig. 14. *R*-phase capacitor voltage and machine current at 5 Hz. Ch1: Capacitor voltage, 50 V/div; Ch2: machine current, 10 A/div; time scale, 50 ms/div.

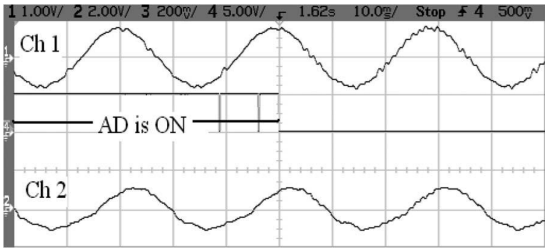

Fig. 15. *R*-phase capacitor voltage and machine current at 35 Hz. Ch1: Capacitor voltage, 500 V/div; Ch2: machine current, 20 A/div; time scale, 10 ms/div.

Table III). It is clearly observed from the waveforms that, after activation of the AD loop in the control, the capacitor voltage waveforms become oscillation free.

Experimental Results at the 2.4-kHz Switching Frequency:

Figs. 12 and 13 are the experimental results for the same

Fig. 16. *R*-phase capacitor voltage and machine current during the sudden speed change from 2.5 to 43 Hz with AD. Ch1: Capacitor voltage, 50 V/div; Ch2: machine current, 20 A/div; Ch3: machine speed, 1500 r/min/div; Ch4: zoomed waveform of the capacitor voltage during the transient speed change; time: 500 ms/div.

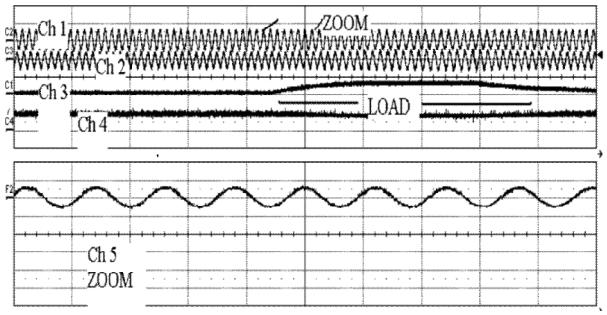

Fig. 17. *R*-phase capacitor voltage and machine current during the sudden application of the 1-kW load at 43 Hz with AD. Ch1: Capacitor voltage, 250 V/div, Ch2: machine current, 20 A/div; Ch3: load, 1.5 kW/div; Ch4: machine speed, 1500 r/min; Ch5: zoomed capacitor voltage during the sudden application of load, 250 V/div; time: 200 ms/div.

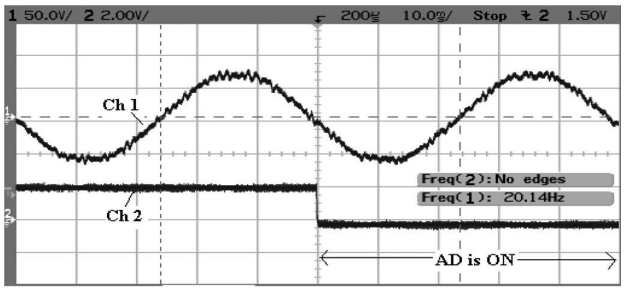

(a)

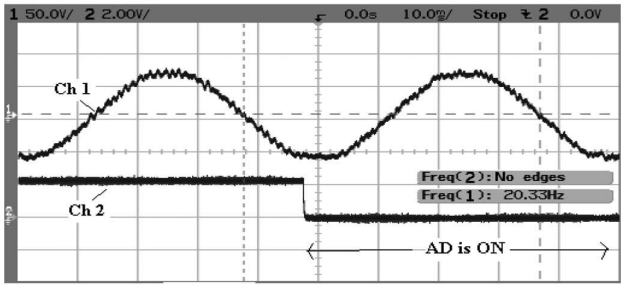

(b)

Fig. 18. (a) *R*-phase capacitor voltage and machine current at 20 Hz (ξ = 0.25) with and without AD. Ch1: Capacitor voltage, 50 V/div; time, 10 ms/div.

(b) *R*-phase capacitor voltage and machine current at 20 Hz (ξ = 0.35) with and without AD. Ch1: Capacitor voltage, 50 V/div; time, 10 ms/div.

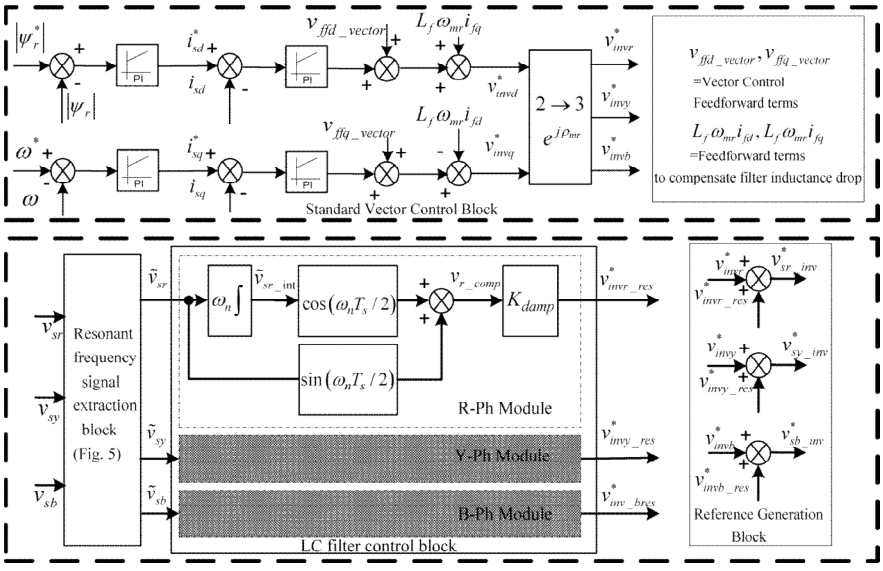

Fig. 19. Complete control block diagram.

machine and the same *LC* filter but with the inverter switching frequency at 2.4 kHz. The phase advancement provided to compensate the inverter delay is 61.1° (as shown in Table III).

B. Experimental Results for a Synchronous Machine (Steady State)

The experiment is carried out using a three-level IGBT-based VSI, and the control algorithm is

implemented on the TMS320LF 2407A digital platform.

Figs. 14 and 15 are the experimental results on a synchronous machine. The machine and filter details are provided in the Appendix and in Table II. The inverter is switched for these experiments at 4.9 kHz, and the system resonant frequency is at 503 Hz. The phase advancement given to compensate the inverter delay is 18.6° (as shown in Table III); results are given for the damping factor $\xi = 0.3$.

The result demonstrates the effectiveness of the method to reduce the resonant-frequency components in the synchronous machine terminal voltages.

C. Experimental Results for an Induction Machine (Dynamic Waveform)

Fig. 16 demonstrates the waveform for a sudden speed change of the machine from 2.5 to 43 Hz with AD. Fig. 17 demonstrates the waveform for a sudden load change at 43 Hz. From these waveforms, it is clear that the AD loop does not affect the dynamic operation of the normal vector control.

This technique only removes the resonant-frequency oscillation from the waveforms.

These experiment results on an induction machine during dy-namic condition demonstrate that the presence of the proposed AD technique does not affect the normal functioning of the field-oriented control.

D. Experimental Results for an Induction

Machine (Robustness)

Fig. 18(a) and (b) is the capacitor voltage waveforms for the damping factor ξ at 0.25 and 0.35, respectively. It can be observed from the experimental results that the small variations of ξ due to the variation of leakage inductance do not disturb the system operation (see Fig. 19).

V. Conclusion

An AD technique has been proposed for vector-controlled CSI-fed ac machine drives with *LC* filters. This technique re-duces resonant-frequency oscillation in motor terminal voltages and line currents. The proposed technique independently works from the vector control loops. The AD technique uses capacitor voltages to construct compensating signals. It acts on a per-phase basis for better accuracy of the control and instantly acts. The proposed AD technique does not work well for very low in-verter switching frequency (around 500 Hz). This technique can be extended to any three-phase *LC*-filter-based system, namely, *LCL*-filter-based front-end converters or shunt active filters.

Appendix

Induction Machine Details

1.1. *Machine details*: *1.5-kW 220-V 11-A 1440-r/min four-pole Y-connected 50-Hz induction machine*;

1.2. *Machine parameters*: $R_s = 0.66\ \Omega$, $R_r = 0.21\ \Omega$, $L_{lr} = 1.62$ mH, $L_{ls} = 1.62$ mH, and $L_m = 38.8$ mH;

1.3. *Filter parameters*: $L_f = 2$ mH, $C_f = 30\ \mu$F, and $f_n =$ 828 Hz.

Synchronous Machine Details

2.1. *Machine details*: *15.8-HP three-phase 400-V 18.3-A 1000-r/min 50-Hz salient-pole wound-field*

synchronous machine;

2.2. *Field Circuit*: 17 V, 13.8 A, R_{sf} = 1.2 Ω, and L_{sf} = 750 mH;

2.3. *Armature Circuit*: R_a = 0.45 Ω, L_{md} = 42.54 mH, L_{mq} = 26.35 mH, and L_{ls} = 7.7 mH;

2.4. *Filter parameters*: L_f = 5 mH, C_f = 20 μF, and f_n = 503 Hz.

References

[1] S. Ogasawara, H. Ayano, and H. Akagi, "Measurement and reduction of EMI radiated by a PWM inverter-fed ac motor drive system," *IEEE Trans. Ind. Appl.*, vol. 33, no. 4, pp. 1019–1026, Jul./Aug. 1997.

[2] F. Wang, "Motor shaft voltages and bearing currents and their reduc-tion in multilevel medium-voltage PWM voltage-source-inverter drive applications," *IEEE Trans. Ind. Appl.*, vol. 36, no. 5, pp. 1336–1341, Sep./Oct. 2000.

[3] S. Chen, T. A. Lipo, and D. Fitzgerald, "Source of induction motor bear-ing currents caused by PWM inverters," *IEEE Trans. Energy Convers.*, vol. 11, no. 1, pp. 25–32, Mar. 1996.

[4] A. H. Bonnett, "Analysis of the impact of pulse-width modulated inverter voltage waveforms on ac induction motors," *IEEE Trans. Ind. Appl.*, vol. 32, no. 2, pp. 386–392, Mar./Apr. 1996.

[5] A. Muetze and A. Binder, "Calculation of circulating bearing currents in machines of inverter-based drive systems," *IEEE Trans. Ind. Electron.*, vol. 54, no. 2, pp. 932–938, Apr. 2007.

[6] A. F. Moreira, P. M. Santos, T. A. Lipo, and G. Venkataramanan, "Filter networks for long cable drives and their influence on motor voltage distri-bution and common-mode currents," *IEEE Trans. Ind. Electron.*, vol. 52, no. 2, pp. 515–522, Apr. 2005.

[7] U. T. Shami and H. Akagi, "Experimental discussions on a shaft end-to-end voltage appearing in an inverter-driven motor," *IEEE Trans. Ind. Electron.*, vol. 24, no. 6, pp. 1532–1540, Jun. 2009.

[8] H. Akagi and S. Tamura, "A passive EMI filter for eliminating both bear-ing current and ground leakage current from an inverter-driven motor," *IEEE Trans. Ind. Electron.*, vol. 21, no. 5, pp. 1459–1469, Sep. 2006.

[9] M. C. Di Piazza, G. Tinè, and G. Vitale, "An improved active common-mode voltage compensation device for induction motor drives," *IEEE Trans. Ind. Electron.*, vol. 55, no. 4, pp. 1823–1834, Apr. 2008.

[10] X. Chen, D. Xu, F. Liu, and J. Zhang, "A novel inverter-output passive filter for reducing both differential- and common-mode *dv/dt* at the mo-tor terminals in PWM drive systems," *IEEE Trans. Ind. Electron.*, vol. 54, no. 1, pp. 419–426, Feb. 2007.

[11] G. Mondal, K. Sivakumar, R. Ramchand, K. Gopakumar, and E. Levi, "A dual seven-level inverter supply for an open-end winding induction motor drive," *IEEE Trans. Ind. Electron.*, vol. 56, no. 5, pp. 1665–1673, May 2009.

[12] S. Mukherjee and G. Poddar, "Fast control of filter for sensorless vector control SQIM drive with sinusoidal motor voltage," *IEEE Trans. Ind. Electron.*, vol. 54, no. 5, pp. 2435–2442, Oct. 2007.

[13] J. K. Steinke, "Use of an *LC* filter to achieve a motor-friendly per-formance of the PWM voltage source inverter," *IEEE Trans. Energy Convers.*, vol. 14, no. 3, pp. 649–654, Sep. 1999.

[14] M. Kojima, K. Hirabayashi, Y. Kawabata, E. C. Ejiogu, and T. Kawabata, "Novel vector control system using deadbeat-controlled PWM inverter with output *LC* filter," *IEEE Trans. Ind. Appl.*, vol. 40, no. 1, pp.

162– 169, Jan./Feb. 2004.

[15] J. Salomaki, M. Hinkkanen, and J. Luomi, "Sensorless control of induc-tion motor drives equipped with inverter output filter," *IEEE Trans. Ind. Electron.*, vol. 53, no. 4, pp. 1188–1197, Aug. 2006.

[16] A. Sapin, P. K. Steimer, and J.-J. Simond, "Modeling, simulation, and test of a three-level voltage-source inverter with output *LC* filter and direct torque control," *IEEE Trans. Ind. Appl.*, vol. 43, no. 2, pp. 469–475, Mar./Apr. 2007.

[17] M. Malinowski and S. Bernet, "A simple voltage sensorless active damping scheme for three-phase PWM converters with an *LCL* filter," *IEEE Trans. Ind. Electron.*, vol. 55, no. 4, pp. 1876–1880, Apr. 2008.

[18] V. Blasko and V. Kaura, "A novel control to actively damp resonance in input *LC* filter of a three-phase voltage source converter," *IEEE Trans. Ind. Electron.*, vol. 33, no. 2, pp. 542–550, Mar./Apr. 1997.

[19] M. Liserre, A. Dell'Aquila, and F. Blaabjerg, "Genetic algorithm-based design of the active damping for an *LCL*-filter three-phase active recti-fier," *IEEE Trans. Power Electron.*, vol. 19, no. 1, pp. 76–86, Jan. 2004.

[20] E. Wu and P. W. Lehn, "Digital current control of a voltage source converter with active damping of *LCL* resonance," *IEEE Trans. Power Electron.*, vol. 21, no. 5, pp. 1364–1373, Sep. 2006.

[21] Y. W. Li, "Control and resonance damping of voltage-source and current-source converters with *LC* filters," *IEEE Trans. Ind. Electron.*, vol. 56, no. 5, pp. 1511–1521, May 2009.

[22] J. C. Wiseman and B. Wu, "Active damping control of a high-power PWM current-source rectifier for line-current THD reduction," *IEEE Trans. Ind. Electron.*, vol. 52, no. 3, pp. 758–764, Jun. 2005.

[23] P. Cortés, G. Ortiz, J. I. Yuz, J. Rodr´guez, S. Vazquez, and L. G. Franquelo, "Model predictive control of an inverter with output *LC* filter for UPS applications," *IEEE Trans. Ind. Electron.*, vol. 56, no. 6, pp. 1875–1883, Jun. 2009.

[24] A. M. Rahimi and A. Emadi, "Active damping in dc/dc power elec-tronic converters: A novel method to overcome the problems of constant power loads," *IEEE Trans. Ind. Electron.*, vol. 56, no. 5, pp. 1428–1439, May 2009.

[25] K. Jalili and S. Bernet, "Design of *LCL* filters of active-front-end two-level voltage-source converters," *IEEE Trans. Ind. Electron.*, vol. 56, no. 5, pp. 1674–1689, May 2009.

[26] B. Wu, *High-Power Converters and AC Drives*. Piscataway, NJ: IEEE Press, 2006.

pp. S. Mariéthoz and M. Morari, "Explicit model-predictive control of a PWM inverter with an *LCL* filter," *IEEE Trans. Ind. Electron.*, vol. 56, no. 2, 389–399, Feb. 2009.

[27] T. Laczynski, T. Werner, and A. Mertens, "Active damping of *LC* -filters for high power drives using synchronous optimal pulsewidth modulation," in *Proc. IEEE Power Electron. Spec. Conf.*, 2008, pp. 1033–1040.

pp. P. A. Dahono, "A control method to damp oscillation in the input *LC* filter," in *Proc. IEEE Power Electron. Spec. Conf.*, 2002, vol. 4, 1630–1635.

[28] P. A. Dahono, "A control method for dc–dc converter that has an *LCL* output filter based on new virtual capacitor and resistor concepts," in *Proc. IEEE Power Electron. Spec. Conf.*, 2004, vol. 1, pp. 36–42.

[29] S. Yang, Q. Lei, F. Z. Peng, and Z. Qian, "A robust control scheme for grid-connected voltage-source inverters," *IEEE Trans. Ind. Electron.*, vol. 58, no. 1, pp. 202–212, Jan. 2011.

[30] G. Shen, X. Zhu, J. Zhang, and D. Xu, "A new feedback method for PR current control of *LCL*-filter based grid-connected inverter," *IEEE Trans. Ind. Electron.*, vol. 57, no. 6, pp. 2033–2041, Jun. 2010.